Electronic Supplementary Material (ESI) for Journal of Materials Chemistry A.
This journal is © The Royal Society of Chemistry 2020

Supporting Information

Ultrafine Phosphorus-Doped Rhodium for Enhanced Hydrogen Electrolysis in Alkaline Electrolyte

*Lixin Su,[a†] Yuanmeng Zhao,[a†] Fulin Yang,[a†] Tian Wu,[c] Gongzhen Cheng,[a] and Wei Luo[a,b]**

[a]College of Chemistry and Molecular Sciences, Wuhan University, Wuhan 430072, P. R. China
[b]Suzhou Institute of Wuhan University, Suzhou, Jiangsu 215123, P. R. China
E-mail: wluo@whu.edu.cn
[c]Institute of Materials Research and Engineering, Hubei University of Education, Wuhan 430205, P. R. China
†These authors contributed equally to this work.

EXPERIMENTAL SECTION

Chemicals and Materials.

Rhodium (III) acetylacetonate ($Rh(acac)_3$, Changcheng Chemical, > 99%), trioctylphosphine (TOP, Aladdin Industrual, 90%), oleylamine (OAm, Aladdin Industrual, 80 ~ 90%), 1-octadecene (ODE, Aladdin Industrual, > 90%), hexane (Sinopharm Chemical Reagent, ≥ 97%), absolute ethanol (Sinopharm Chemical Reagent, ≥ 99.7%), sulfuric acid (H_2SO_4, Sinopharm Chemical Reagent, 95.0 ~ 98.0%), copper (II) sulfate pentahydrate ($CuSO_4·5H2O$, Sinopharm Chemical Reagent, ≥ 99.0%), potassium hydroxide (KOH, Aladdin Industrual, 99.999% metals basis, except sodium), isopropanol (Sinopharm Chemical Reagent, ≥ 99.7%), Nafion® 117 solution (Sigma-Aldrich, ~ 5% in a mixture of lower aliphatic alcohols and water), and Pt/C (Johnson Matthey Hispec 3600, Shanghai Hesen Electric, 20%) were utilized directly without any further purification. The ultrapure water (18.25 MΩ cm^{-1}) prepared from an up water purification system (Ulupure) was used throughout the whole experiment.

Synthesis of P-Rh/C.

4.0 mL of OAm and 40.0 mg of Vulcan carbon powder (XC-72) were added to a three-neck flask and stirred magnetically. Then the temperature of solution was increased to 120 °C and kept for 30 min under vacuum to remove the moisture and oxygen in the reaction system. After the solution was refilled with nitrogen, 1.0 mL of TOP was injected to the solution, and the temperature was further raised. When the solution was heated to 360 °C, 40.0 mg of $Rh(acac)_3$ dissolved in 2.0 mL of OAm were injected to the solution and maintained at this temperature for 120 min. The resulting solution was

subsequently cooled to room temperature naturally, and the obtained P-Rh/C samples were collected by centrifugation with adding n-hexane and ethanol. Afterwards, the obtained product was dried at room temperature under vacuum. Finally, the dried samples were put in a quartz boat in the center of a tube furnace and annealed under a gas atomosphere (5% H_2, 95% N_2) at 400 °C or 600 °C for 60 min. The temperature of tube furnace was raised at a rate of 5 °C min^{-1}.

Synthesis of Rh/C.

40.0 mg of $Rh(acac)_3$, 3.0 mL of OAm, 3.0 mL of ODE, and 40.0 mg of XC-72 were added to a three-neck flask and stirred magnetically. Then the solution was heated to 120 °C and kept for 30 min under vacuum. After the solution refilled with nitrogen, the temperature was raised to 280 °C and maintained at this temperature for 120 min. The resulting solution was then cooled to room temperature, and the obtained Rh/C samples were collected by centrifugation with adding n-hexane and ethanol. Then the obtained product was dried at room temperature under vacuum. Finally, the dried samples were annealed in a tube furnace under a gas atomosphere (5% H_2, 95% N_2) at 400 °C for 60 min.

Materials characterization.

The X-ray powder diffraction (XRD) patterns were obtained on a Rigaku Miniflex600 X-ray powder diffractometer equipped with a Cu Kα radiation source (λ = 0.154178 nm). All of the diffraction data were collected in a 2θ range from 20° to 80° at a scanning rate of 8° min^{-1}. The transmission electron microscopy (TEM) observation and the energy dispersive spectroscopy (EDS) data were performed using a FEI Tecnai

G20 U-Twin transmission electron microscope equipped with an EDX spectrometer at an acceleration voltage of 200 kV. High resolution TEM (HRTEM) images and high angle annular dark field scanning transmission electron microscopy(HAADF-STEM) images were conducted on a Titan G2 60-300 transmission electron microscope operated at an acceleration voltage of 300 kV. X-ray photoelectron spectroscopy (XPS) measurement was performed with a Kratos XSAM 800 spectrophotometer. Inductively coupled plasma atomic emission spectroscopy (ICP-AES) was performed on a Thermo IRIS Intrepid II XSP atomic emission spectrometer.

Preparation of working electrodes.

For hydrogen evolution reaction (HER), 5.0 mg of P-Rh/C (400 °C), P-Rh/C (600 °C), Rh/C, or commercial Pt/C was mixed with 1 mL of isopropanol solvent containing 0.1 wt% Nafion and ultrasonicated for 30 min to form a homogeneous ink. The glassy carbon (GC) electrode with a diameter of 5 mm was polished with 1.0, 0.5 and 0.05 mm gamma alumina powder slurry, and rinsed with ultrapure water and ethanol to obtain a neat surface. When the GC electrode was dried under air naturally, 6 μL ink was drop-casted on the surface of the GC electrode and dried in air before any electrochemical measurements. Compared with HER, the preparation for the working electrode of hydrogen oxidation reaction (HOR) only differed in the loading. 4.0 mg catalyst powders were mixed with 2 mL of isopropanol solvent containing 0.025 wt% Nafion and 5 μL ink was drop-casted on the surface of the GC electrode. The metal loadings on electrode were calculated from the ICP-AES data.

Electrochemical Measurements.

Electrochemical tests were conducted at CHI 760E electrochemistry workstation. The GC electrode decorated by electrocatalyst served as the working electrode, and the graphite rod with a diameter of 5 mm served as the counter electrode as well as the saturated calomel electrode (SCE) and the Hg/HgO electrode was used as reference electrode. In this study, all operation was performed at the constant temperature at 303 (± 0.1) K, and all the measured potentials were referred to the reversible hydrogen electrode (RHE) potential with *iR*-compensation. For HER, the catalysts were pre-treated under Ar-saturated 1.0 M KOH by cyclic voltammetry (CV) curves to obtain a stable voltammogram. Then, the polarization curve was recorded by a rotating disk electrode (RDE) system (Pine Research Instruments) with the rotation rate of 1600 revolutions per minute (rpm) at a scan rate of 5 mV s^{-1} in Ar-saturated 1.0 M KOH. For HOR evaluation, the catalysts were also pre-treated under Ar-saturated 0.1 M KOH by cyclic voltammetry (CV) curves from ~ 0.02 to 1.12 V for Rh/C and Pt/C and from ~ 0.02 to 0.72 V for P-Rh/C to obtain a stable voltammogram. After the fresh electrolyte was H_2-saturated, the polarization curve was performed in the potential range from about −0.08 to 1.12 V for Rh/C and Pt/C and about −0.08 to 0.72 V for P-Rh/C at a scan rate of 10 mV s^{-1} under the RDE rotation rate of 1600 rpm. Accelerated durability test (ADT) was operated by 1000 CV cycles under Ar-saturated electrolyte for both HER and HOR.

Electrochemically active surface areas (ECSAs) were tested by Cu underpotential deposition (Cu_{UPD}) stripping. Typically, CV on each catalyst was first carried out at a scan rate of 10 mV s^{-1} in Ar-purged 0.1 M H_2SO_4 solution to obtain a steady

voltammogram as the background. Then, Cu_{UPD} stripping was performed at a scan rate of 10 mV s^{-1} in Ar-purged 0.1 M H_2SO_4 solution containing 2 mM $CuSO_4$ after Cu deposition at about 0.30 V for 100 s, with the potential beginning from about 0.30 V. The value of ECSA ($cm^2\ \mu g_{metal}^{-1}$) can be calculated by Eq. S1,

$$ECSA = \frac{Q_{Cu}}{Q_s \cdot m_{metal}} \quad \text{Eq. S1}$$

Where Q_{Cu} is the measured integral charge (420 μC cm^{-2}, $Cu_{UPD} \rightarrow Cu^{2+} + 2e^-$), Q_s is the surface charge density of 420 μC cm_{metal}^{-2} which is assumed for a monolayer adsorption of Cu_{UPD} on metal.

Electrochemical impedance spectra (EIS) tests were conducted with the AC impedance spectra from 200 kHz to 0.1 kHz and a voltage perturbation of 10 mV. The real part of the resistance at 1 kHz was taken as the uncompensated resistance (R_u) and was used to obtain the *iR*-free potential ($E_{iR\text{-free}}$) according to the following equation (Eq. S2),

$$E_{iR-free} = E - iR_u \quad \text{Eq. S2}$$

where E is the measured potential and i is the corresponding current.

Nernstian diffusion overpotential (η_{diff}) could be calculated from Eq. S3,

$$\eta_{diff} = -\frac{RT}{nF}\left(1 - \frac{j}{j^d}\right) \quad \text{Eq. S3}$$

where R, T, F, n, and j^d are the universal gas constant (8.314 J mol^{-1} K^{-1}), the temperature in Kelvin (303 K), the Faraday constant, the electron transfer number, and the hydrogen diffusion limited current density, respectively.

Kinetic current density (j^k) could be deduced from the Koutecky-Levich equation (Eq. S4),

$$\frac{1}{j} = \frac{1}{j^k} + \frac{1}{j^d} = \frac{1}{j^k} + \frac{1}{Bc_0\omega^{1/2}} \quad \text{Eq. S4}$$

where j, B, c_0, and ω are the measured current density, the Levich constant, the solubility of H_2 (7.33×10^{-4} mol L^{-1}), and the speed of the rotating, respectively.

Exchange current density (j^0) could be extracted from the Butler-Volmer equation (Eq. S5),

$$j^k = j^0\left[e^{\frac{\alpha F}{RT}\eta} - e^{\frac{-(1-\alpha)F}{RT}\eta}\right] \quad \text{Eq. S5}$$

j^0 could be also obtained from the approximate Butler-Volmer equation (Eq. S6),

$$j = j^0\frac{\eta F}{RT} \quad \text{Eq. S6}$$

where α and η represent the transfer coefficient and the overpotential, respectively.

DFT Calculations.

All the DFT calculations in this paper were performed using the CASTEP module in Material Studio program. The generalized gradient approximation method (GGA) with the Perdew-Burke-Ernzerh (PBE) functional was used to describe the exchange and correlation interactions.[1,2] The interactions between valence electrons and ionic cores was described by Ultrasoft pseudo-potential. 6×6×1 Monkhorst-Pack grid k-points are employed for P-Rh and Rh geometric optimization. The convergence threshold is set as 1.0e-6 eV in energy and 0.03 eV/Å in force, respectively. The electronic wave functions were expanded on a plane wave basis with a cut-off energy of 400 eV. We choose (111) surface as the model of P-Rh and Rh for calculation, with a vacuum gap of ~15 Å. The adsorption free energies were determined by the following formula $\Delta G = \Delta E + \Delta ZPE - T\Delta S$, where ΔE, ΔZPE and ΔS represent the binding energy, zero point

energy change and entropy change of the adsorption of adsorbates, respectively. The related zero point energies and entropies of H_2, H_2O, H* and OH* are from previous literatures.[3]

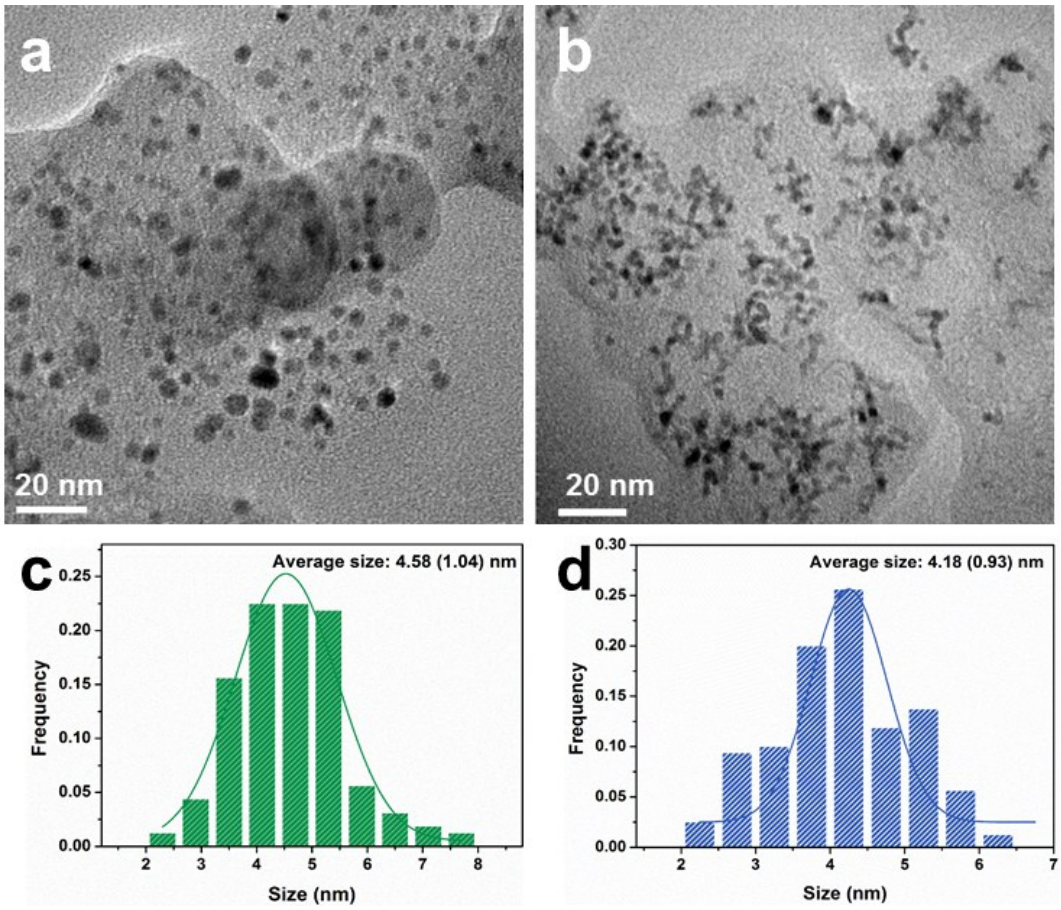

Figure S1. TEM images of (a) P-Rh/C (600 °C), (b) Rh/C. Size distribution histogram of (c) P-Rh/C (600 °C), (d) Rh/C.

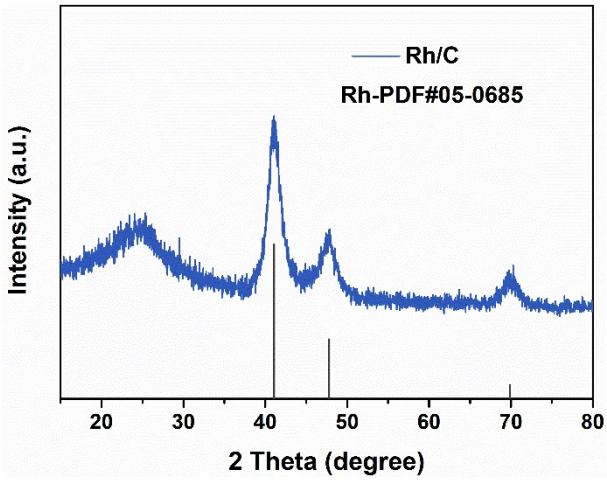

Figure S2. XRD pattern of Rh/C.

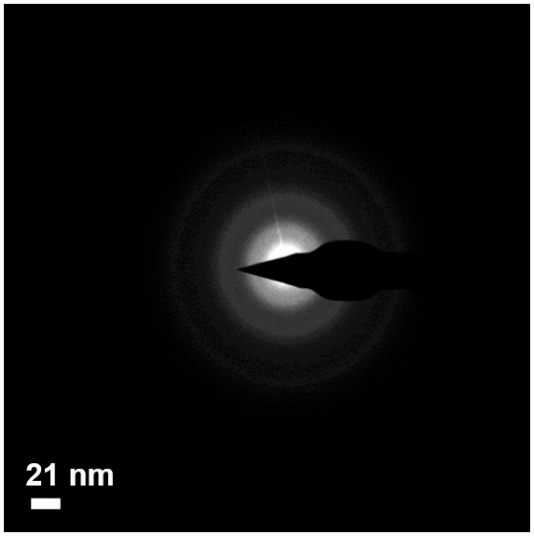

Figure S3. SAED pattern of P-Rh/C (400 °C).

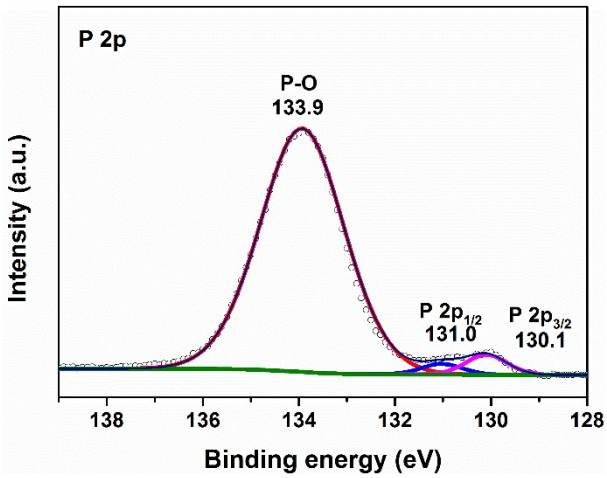

Figure S4. High resolution XPS of P 2p in P-Rh/C (400 °C).

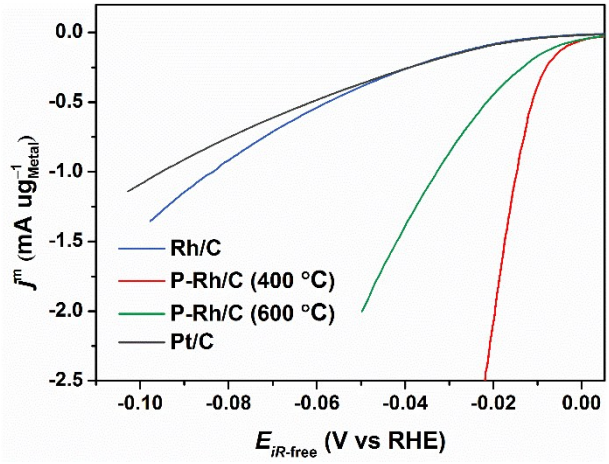

Figure S5. HER polarization curves obtained in Ar-saturated 1.0 M KOH with a rotation speed of 1600 rpm at a scan rate of 5 mV s^{-1}. The current density normalized by the metal mass.

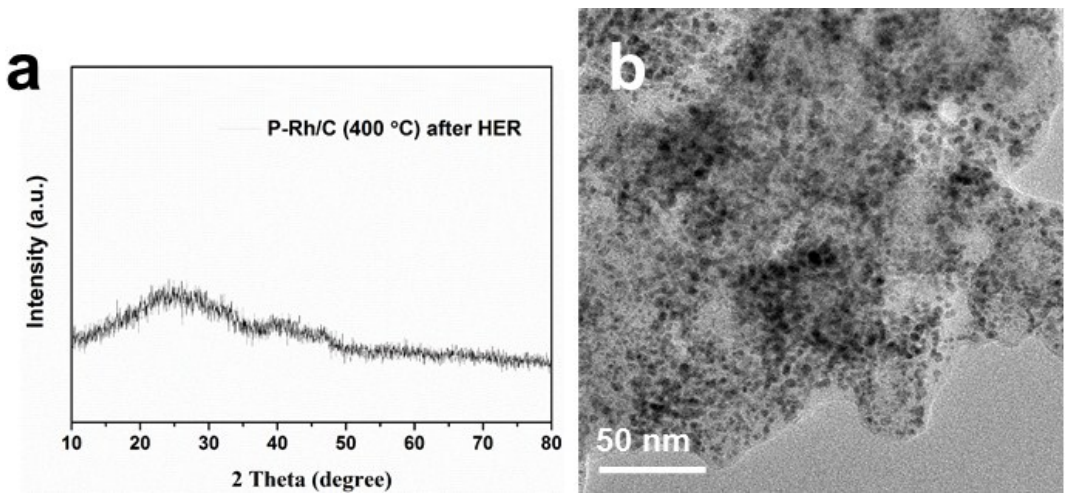

Figure S6. XRD pattern (a), TEM image (b) of P-Rh/C (400 °C) after 1000 CV cycles in Ar-saturated 1.0 M KOH.

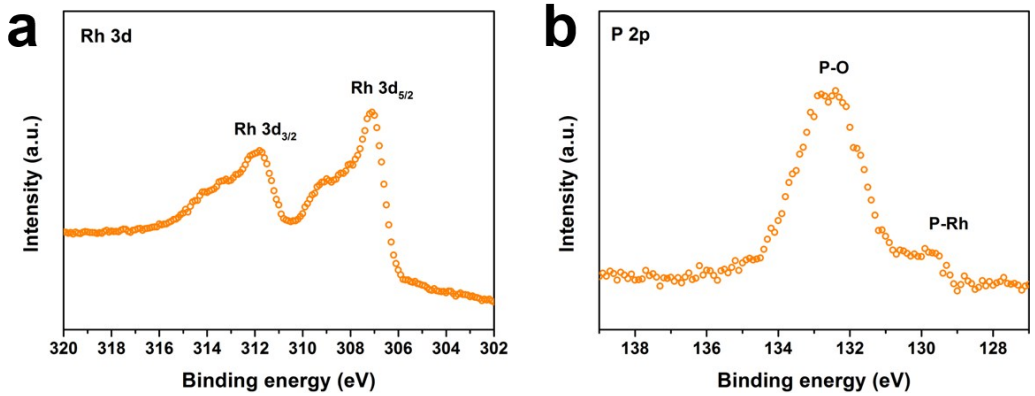

Figure S7. High resolution XPS of (a) Rh 3d, (b) P 2p in P-Rh/C (400 °C) after 1000 CV cycles.

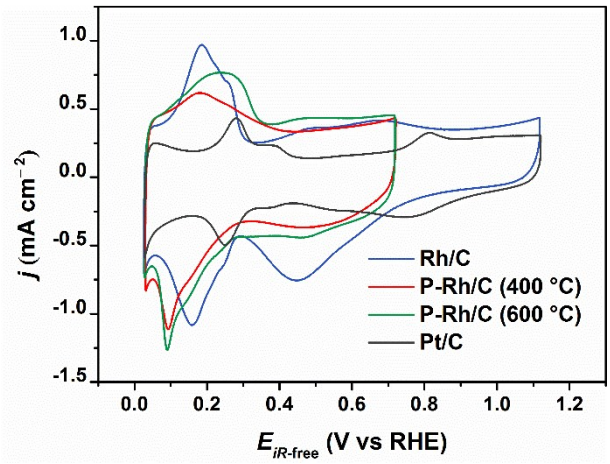

Figure S8. CV curves of Rh/C, P-Rh/C (400 °C), P-Rh/C (600 °C) and Pt/C conducted in Ar-saturated 0.1 M KOH at a scan rate of 50 mV s^{-1}.

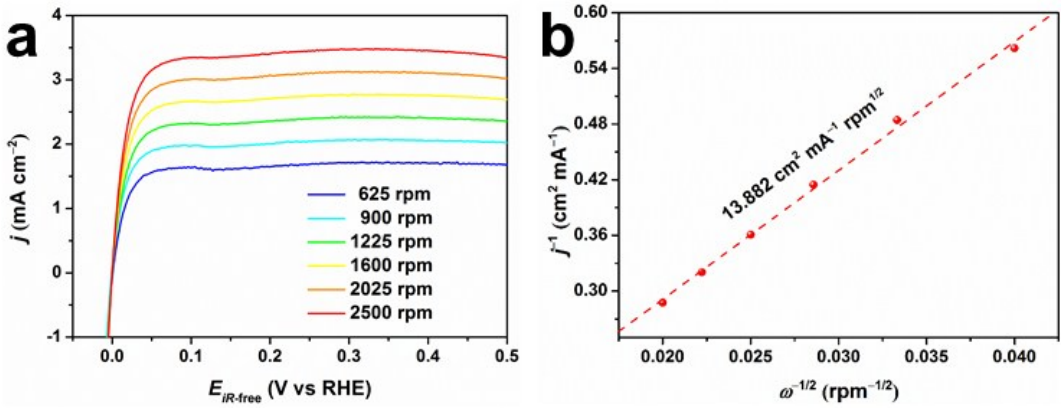

Figure S9. (a) HOR polarization curves of P-Rh/C (400 °C) in H_2-saturated 0.1 M KOH with a scan rate of 10 mV s^{-1} at the rotating speeds varied from 2500 to 625 rpm. (b) Koutecky–Levich plot obtained from (a) at an overpotential of 350 mV. The slope ($1/Bc_0$) is 13.882 cm^2 mA^{-2} $rpm^{1/2}$.

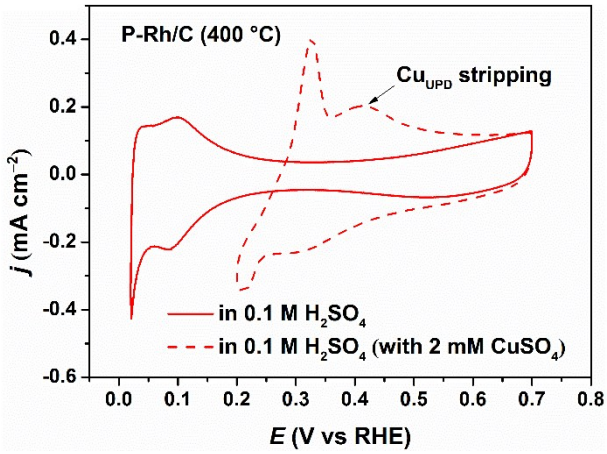

Figure S10. CVs of P-Rh/C (400 °C) in Ar-saturated 0.1 M H_2SO_4 with or without 2 mM $CuSO_4$ at a scan rate of 10 mV s^{-1}. The anodic peak (arrow) corresponds to Cu_{UPD} peak.

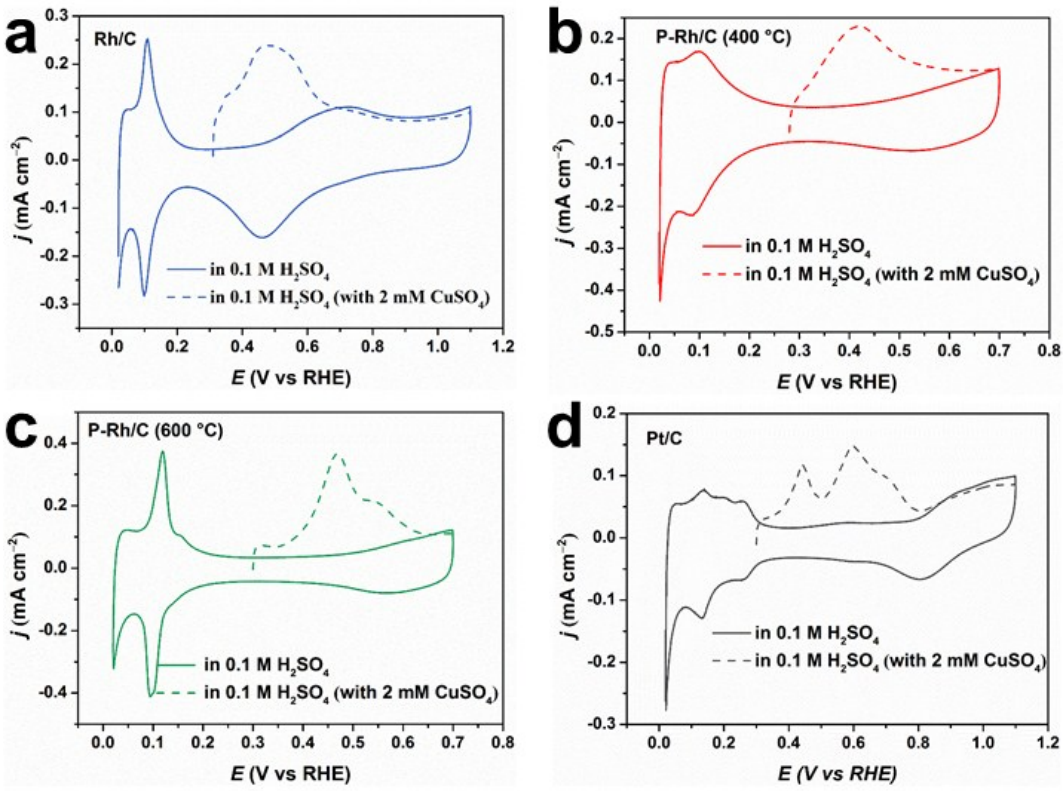

Figure S11. CVs (solid lines) and Cu_{UPD} stripping voltammograms (dash lines) of (a) Rh/C, (b) P-Rh/C (400 °C), (c) P-Rh/C (600 °C) and (d) Pt/C. The Cu deposition at about 0.30 V.

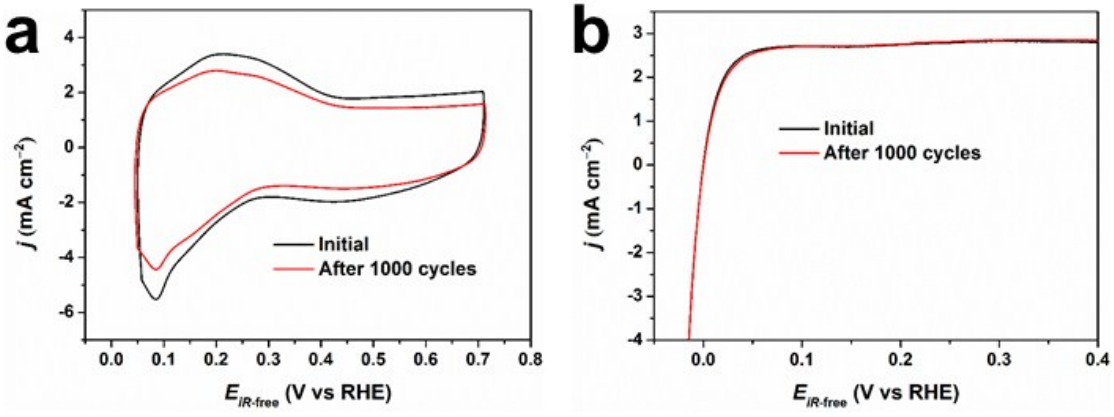

Figure S12. CV curves (a), HOR polarization curves (b) of P-Rh/C (400 °C) recorded before and after 1000 cycles in 0.1 M KOH. The metal mass loading on GC electrode in P-Rh/C (400 °C) was 25.64 μg cm^{-2}.

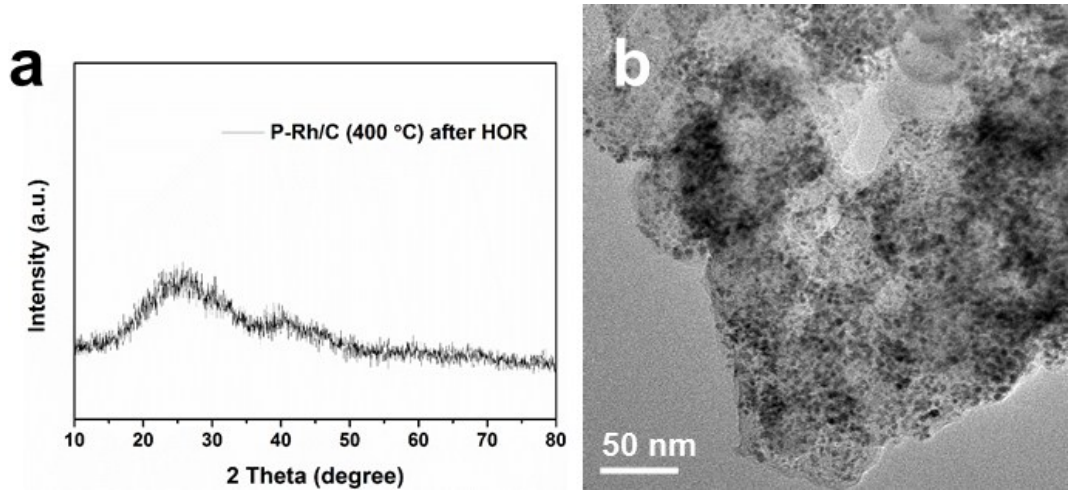

Figure S13. XRD graph (a), TEM image (b) of P-Rh/C (400 °C) after 1000 CV cycles in Ar-saturated 0.1 M KOH.

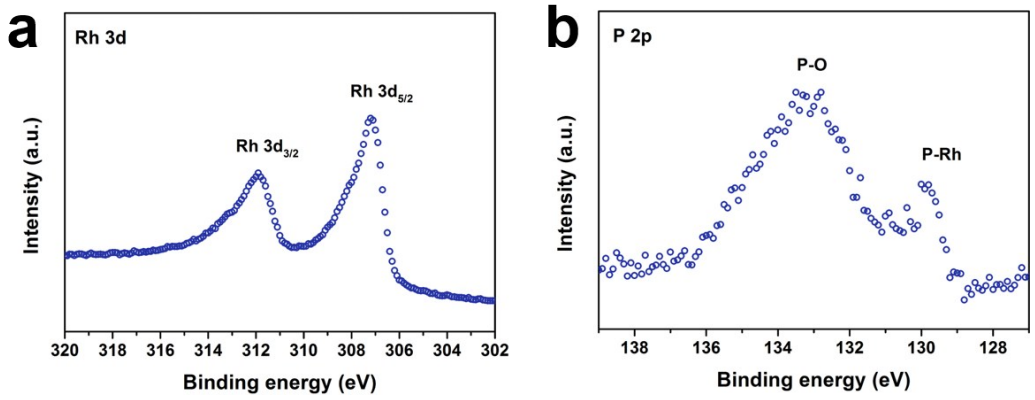

Figure S14. High resolution XPS of (a) Rh 3d, (b) P 2p in P-Rh/C (400 °C) after 1000 CV cycles in Ar-saturated 0.1 M KOH.

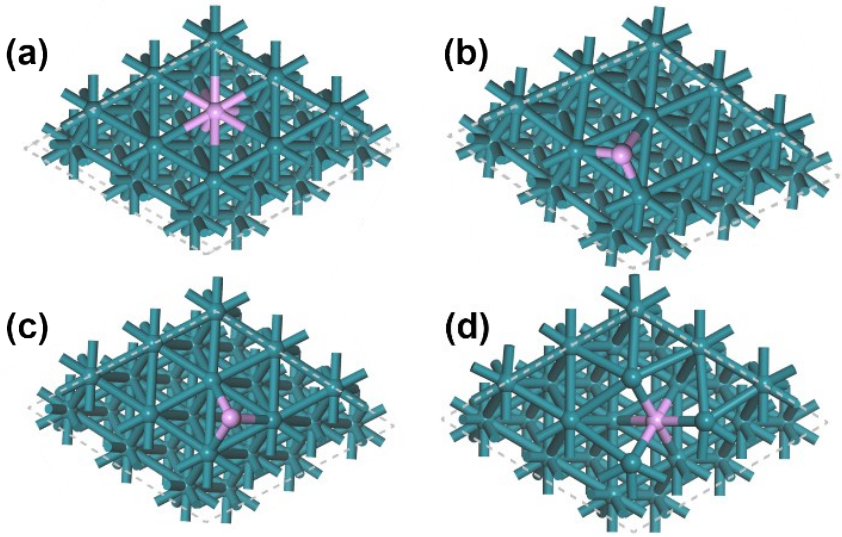

Figure S15. Four different models of P-Rh. These models are P substituted Rh (a), P adsorbed on the surface of Rh (b: hcp-P on Rh surface; c: fcc-P on Rh surface), and P in the interstitial lattice sites of Rh (d).

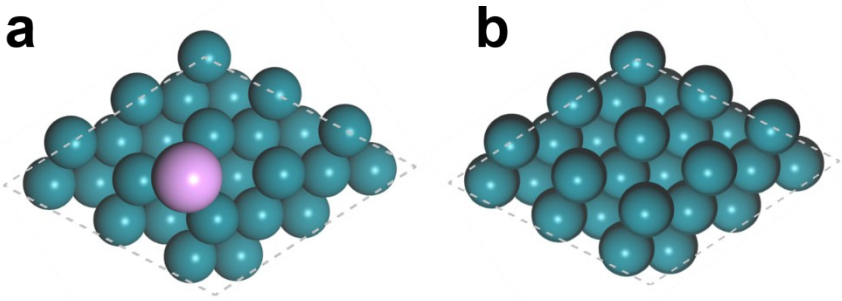

Figure S16. DFT-optimized structure of P-Rh (a) and Rh (b).

Figure S17. The optimized structure models of the adopted adsorption sites of H, H-

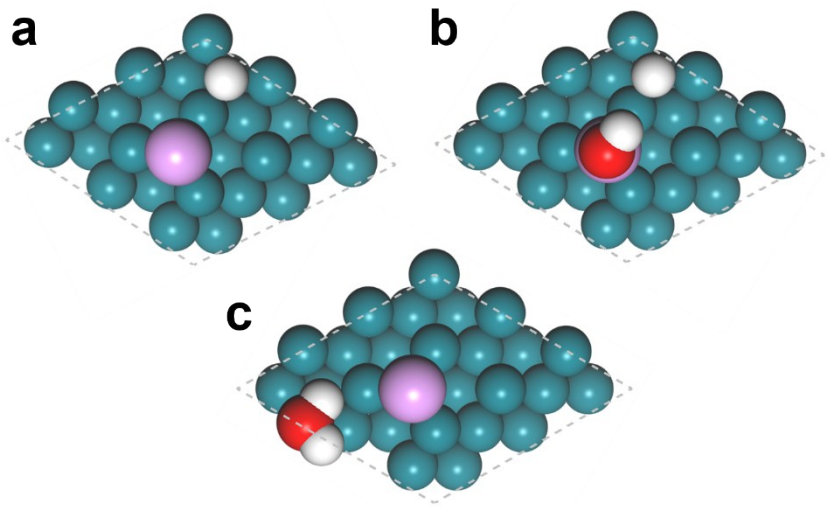

OH and H_2O (a, b and c) on the surface of P-Rh. The cyan, magenta, red and white balls represent Rh, P, O, and H atoms, respectively.

Figure S18. The optimized structure models of the adopted adsorption sites of H, H-

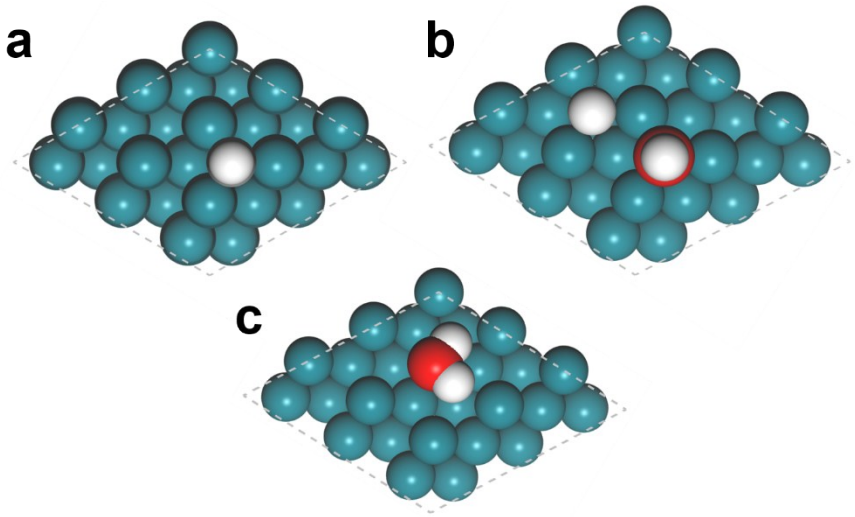

OH and H2O (a, b and c) on the surface of Rh. The cyan, red and white balls represent Rh, O, and H atoms, respectively.

Table S1. ICP-AES data of P-Rh/C (400 °C), P-Rh/C (600 °C) and Rh/C.

Sample	Rh (wt%)	P (wt%)
P-Rh/C (400 °C)	12.57	4.54
P-Rh/C (600 °C)	14.25	3.94
Rh/C	12.94	/

Table S2. Comparison of the HER activity in alkaline medium for P-Rh/C in this work with other precious metal based catalysts reported.

Catalysts	Electrolytes	Overpotential @10 mA cm^{-2} (mV)	Loading (μg_{Metal} cm^{-2})	References
P-Rh/C (400 °C)	**1.0 M KOH**	**11**	**19.23**	**This work**
P-Rh/C (600 °C)		**20**	**21.78**	
RhP_x@NPC	1.0 M KOH	69	/	4
Rh_2P nanoparticles	1.0 M KOH	30	18.7	5
Rh_2P nanocubes	0.1 M KOH	30.8 @5 mA cm^{-2}	3.7	6
Rh_2P nanosheets	0.1 M KOH	18.3	10.7	7
Rh-Rh_2O_3-NPs/C	0.5 M KOH	63	28	8
PdP_2@CB	1.0 M KOH	35.4	17.9	9
IrP_2@NC	1.0 M KOH	28	77	10
IrP_2-rGO	1.0 M KOH	13	8.89	11
Ir ONAs	0.1 M KOH	47	30	12
RuP_2@NPC	1.0 M KOH	52	233	13

Ru/C_3N_4/C	0.1 M KOH	79	~40.8	14
OsP_2@NPC	1.0 M KOH	90	13.9	15
OsP_2@NPC	1.0 M KOH	70	/	16

Table S3. The data of catalysts in this work for HOR.

Sample	Butler-Volmer fitting				Micropolarization	
	α	$j^{0,s}$ (mA cm_{ECSA}^{-2})	$j^{0,m}$ (mA μg_{Metal}^{-1})	$j^{k,m}_{@10mV}$ (mA μg_{Metal}^{-1})	$j^{0,s}$ (mA cm_{ECSA}^{-2}	$j^{0,m}$ (mA μg_{Metal}^{-1})
Rh/C	0.787	0.271	0.433	0.181	0.249	0.398
P-Rh/C (400 °C)	0.798	0.494	0.675	0.292	0.499	0.683
P-Rh/C (600 °C)	0.700	0.303	0.467	0.187	0.310	0.478
Pt/C	0.641	0.340	0.249	0.105	0.363	0.266

The data in the table is the average value calculated from at least three sets of experimental repeats.

Table S4. Comparison of the HOR activity in 0.1 M KOH for P-Rh/C (400 °C) in this work with other precious metal based catalysts reported.

Catalysts	ECSA (cm^2 μg_{Metal}^{-1})	Loading (μg_{Metal} cm^{-2})	$j^{0,s}$ (mA cm_{ECSA}^{-2})	$j^{0,m}$ (mA μg_{Metal}^{-1})	References
P-Rh/C (400 °C)	**1.366**	**6.41**	**0.499**	**0.683**	**This work**
Rh-Rh_2O_3-NPs/C	0.28	28	0.425	0.119	8
Ir NP/PC	0.403	10	0.023	0.009	17
Rh NP/PC	0.995		0.164	0.163	
Pt/C	0.494		0.410	0.203	
Ru NP/PC	1.155		0.227	0.263	
Commercial Rh/C	1.43	10	0.34	0.49	18
$Pd_{0.33}Ir_{0.67}$ nanoparticles	1.06	10	0.45	0.481	19
IrNi@PdIr/C	0.516	19.7	0.209	0.108	20
$Ir_3Pd_1Ru_6$/C	1.21	3.5	0.6	0.73	21
Ir_9Pd_1/C	0.91		0.9	0.82	
Ru–Ir/C-20	0.721	7.8	0.85	0.61	22
Ir ONA/C	0.155	30	0.518	0.080	12

Table S5. The formation energies of different P-doped Rh structures in Figure S15.

Different models	a	b	c	d
Formation energy/eV	-1.14	-1.74	-1.65	-0.82

Reference

1 J. P. Perdew, K. Burke and M. Ernzerhof, *Phys. Rev. Lett*., 1996, **77**, 3865.

2 D. Vanderbilt, *Phys. Rev. B,* 1990, **41**, 7892.

3 J. K. Norskov, T. Bligaard, A. Lagadottir, J. R. Kitchin, J. G. Chen, S. Pandeloy and U. Stimming, *J. Electrochem. Soc.,* 2005, **152**, J23.

4 J. Chi, X. Zeng, X. Shang, B. Dong, Y. Chai, C. Liu, M. Marin and Y. Yin, *Adv. Funct. Mater.*, 2019, **29**, 1901790.

5 F. Yang, Y. Zhao, Y. Du, Y. Chen, G. Cheng, S. Chen and W. Luo, *Adv. Energy Mater.*, 2018, **8**, 1703489.

6 H. Duan, D. Li, Y. Tang, Y. He, S. Ji, R. Wang, H. Lv, P. P. Lopes, A. P. Paulikas, H. Li, S. X. Mao, C. Wang, N. M. Markovic, J. Li, V. R. Stamenkovic and Y. Li, *J. Am. Chem. Soc.*, 2017, **139**, 5494.

7 K. Wang, B. Huang, F. Lin, F. Lv, M. Luo, P. Zhou, Q. Liu, W. Zhang, C. Yang, Y. Tang, Y. Yang, W. Wang, H. Wang and S. Guo, *Adv. Energy Mater.*, 2018, **8**, 1801891.

8 M. K. Kundu, R. Mishra, T. Bhowmik and S. Barman, *J. Mater. Chem. A*, 2018, **6**, 23531.

9 F. Luo, Q. Zhang, X. Yu, S. Xiao, Y. Ling, H. Hu, L. Guo, Z. Yang, L. Huang, W. Cai and H. Cheng, *Angew. Chem. Int. Ed.*, 2018, **57**, 14862.

10 Z. Pu, J. Zhao, I. S. Amiinu, W. Li, M. Wang, D. He and S. Mu, *Energy Environ. Sci.*, 2019, **12**, 952.

11 Z. Pu, T. Liu, W. Zhao, X. Shi, Y. Liu, G. Zhang, W. Hu, S. Sun and S. Liao, *ACS*

Appl. Mater. Interfaces, 2020, **12**, 11737.

12 F. Yang, X. Bao, P. Li, X. Wang, G. Cheng, S. Chen and W. Luo, *Angew. Chem. Int. Ed.*, 2019, **58**, 14179.

13 Z. Pu, I. S. Amiinu, Z. Kou, W. Li and S. Mu, *Angew. Chem. Int. Ed.*, 2017, **56**, 11559.

14 Y. Zheng, Y. Jiao, Y. Zhu, L. H. Li, Y. Han, Y. Chen, M. Jaroniec and S.-Z. Qiao, *J. Am. Chem. Soc.*, 2016, **138**, 16174.

15 S. Chakrabartty, B. K. Barman and C. R. Raj, *Chem. Commun.*, 2019, **55**, 4399.

16 L. Fang, Y. Wang, X. Yang, H. Zhang and Y. Wang, *J. Catal.*, 2019, **370**, 404.

17 M. Ming, Y. Zhang, C. He, L. Zhao, S. Niu, G. Fan and J.-S. Hu, *Small*, 2019, **15**, 1903057.

18 J. Zheng, W. Sheng, Z. Zhuang, B. Xu and Y. Yan, *Sci. Adv.*, 2016, **2**, e1501602.

19 Y. Cong, I. T. McCrum, X. Gao, Y. Lv, S. Miao, Z. Shao, B. Yi, H.Yu, M. J. Janik and Y. Song, *J. Mater. Chem. A*, 2019, **7**, 3161.

20 B. Qin, H. Yu, J. Jia, C. Jun, X. Gao, D. Yao, X. Sun, W. Song, B. Yi and Z. Shao, *Nanoscale*, 2018, **10**, 4872.

21 H. Wang and H. D. Abruna, *J. Am. Chem. Soc.*, 2017, **139**, 6807.

22 J. Ohyama, D. Kumada and A. Satsuma, *J. Mater. Chem. A*, 2016, **4**, 15980.